A General Analysis of Propagation Along Multiple-Layer Superconducting Stripline and Microstrip Transmission Lines

David Nghiem, *Student Member, IEEE*, Jeffery T. Williams, *Member, IEEE*, and David R. Jackson, *Member, IEEE*

Abstract—**A rigorous spectral-domain formulation for a superconducting stripline or microstrip transmission line with a multiple-layer dielectric substrate is presented. The formulation models the strip conductor as a surface current with an equivalent surface impedance, where the surface impedance is approximated in closed form when the strip is either much thinner or much thicker than a penetration depth. In either case the surface impedance is related to the complex conductivity of the material, which is calculated from a two-fluid model. Results are presented to show the slow-wave propagation and attenuation along both microstrip and stripline packages in a realistic multiple-layer configuration, which accounts for the field penetration into the superconducting ground planes.**

I. Introduction

STRIPLINE and microstrip transmission lines are the most common wave-guiding structures used in microwave and millimeter-wave systems. Loss along these transmission lines is due to the ohmic losses of the conductors and dielectric. When constructed of normally conducting materials, the loss for typical designs is due primarily to the ohmic losses of the conductors, particularly at high frequencies. These losses are significantly reduced when superconducting materials are used. Therefore, for long delay lines, large corporate antenna feeds, resonators, and matching circuits, devices for which conductor losses are especially deleterious, high-temperature superconducting materials represent potential alternatives to the normal metals.

To use high-T_c superconductors in high-frequency systems it is important that their special properties be determined and properly accounted for in the design. In the electrical characterization of these superconductors, stripline and microstrip transmission lines and resonators are commonly used. From measurements of the propagation characteristics and the quality factors of these devices, constructed either partially or totally of the superconducting material under test, we can determine many of the macroscopic electrical parameters of the superconductor, such as the surface resistance, conductivity, critical temperature, magnetic field strength, and field penetration depth. This requires correlating the results of analytical and numerical models of the experiment with the measured results. Therefore, it is crucial to have accurate models for the experimental test structures to facilitate the testing and development of empirical material models for the superconductors and to accurately determine the macroscopic electrical parameters of the materials.

Previous investigators have analyzed superconducting microstrip transmission lines [1]–[3]. These investigations have not, however, addressed the stripline structure, and strip width effects have not been explicitly discussed. We will present a rigorous electromagnetic model for the multiple-layer stripline and microstrip from which complex modal propagation constants are calculated. This model will be used to demonstrate the slow wave propagation along superconducting transmission line structures, a result of a large fraction of energy being stored in the superconducting film as the kinetic motion of paired electrons (kinetic inductance). We will also show the functional dependence of the propagation constant/phase velocity on the width of the conducting strip and the effective field penetration depth of the superconductor.

II. Spectral-Domain Formulation

Our analysis of the multiple-layer stripline and microstrip is based on standard spectral-domain techniques. A cross-sectional view of the general transmission line structure is shown in Fig. 1. An electric surface current density, $\boldsymbol{J}(\boldsymbol{r})$, is shown embedded arbitrarily within layer m in this figure for generality, although in practice the strip would typically be at an interface. The total electric field in the mth layer generated by $\boldsymbol{J}(\boldsymbol{r})$ on the conducting strip is written as

$$\boldsymbol{E}(x,y,z) = \int\int \overline{\boldsymbol{G}}(x-x', y-y', z, z_0)\cdot \boldsymbol{J}(x',y')\,dx'\,dy' \tag{1}$$

where the strip is assumed to be infinitesimally thin, located at $z = z_0$, and $\overline{\boldsymbol{G}}$ is the multiple-layer electric

Manuscript received October 17, 1990; revised April 29, 1991. This work was supported by the Texas Center for Superconductivity at the University of Houston, by DARPA under Prime Grant MDA 972-89-J-1001, by the NASA-Johnson Manned Space Center under Grant NAG 9-352, and by the State of Texas.

The authors are with the Department of Electrical Engineering, University of Houston, Houston, TX 77204-4793.

IEEE Log Number 9101268.

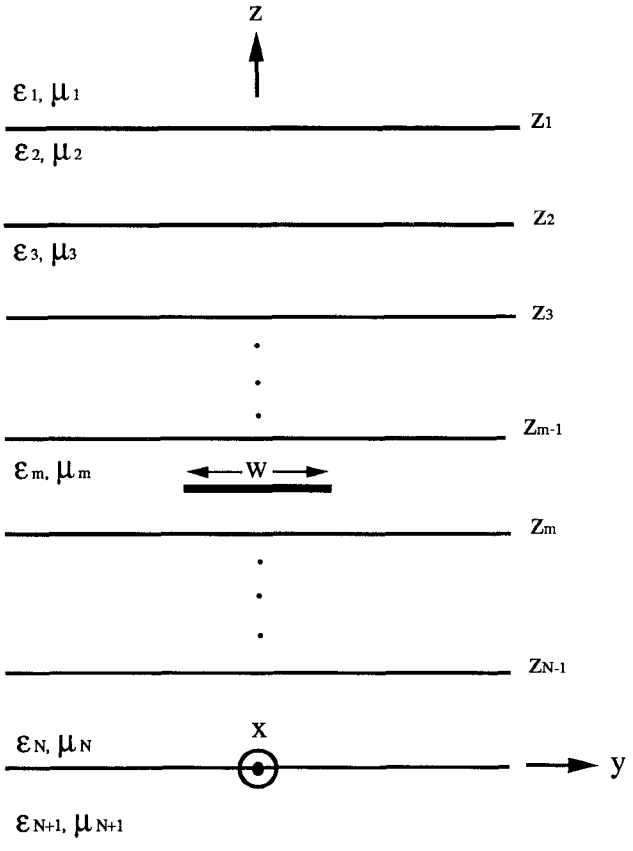

Fig. 1. General multiple-layer transmission line structure.

field dyadic Green's function. In order to simplify the analysis, we assume that the layered structure is infinite along the x and y coordinates, so that the original three-dimensional analysis is reduced to a one-dimensional problem in the spectral domain by utilizing a two-dimensional Fourier transform in x and y. Applying the Fourier-convolution theorem [4], the components of the transformed electric field are expressed as

$$\tilde{E}_x(k_x,k_y,z)=\tilde{G}_{xx}(k_x,k_y,z,z_0)\tilde{J}_x(k_x,k_y)+\tilde{G}_{xy}(k_x,k_y,z,z_0)\tilde{J}_y(k_x,k_y) \quad (2)$$

$$\tilde{E}_y(k_x,k_y,z)=\tilde{G}_{yx}(k_x,k_y,z,z_0)\tilde{J}_x(k_x,k_y)+\tilde{G}_{yy}(k_x,k_y,z,z_0)\tilde{J}_y(k_x,k_y) \quad (3)$$

and

$$\tilde{E}_z(k_x,k_y,z)=\tilde{G}_{zx}(k_x,k_y,z,z_0)\tilde{J}_x(k_x,k_y)+\tilde{G}_{zy}(k_x,k_y,z,z_0)\tilde{J}_y(k_x,k_y). \quad (4)$$

The tilde ($\sim$) over a variable denotes the Fourier transform of that quantity. We will assume that the fields propagate in the positive x direction with a propagation constant k_{x0}; thus, the surface current density, $\boldsymbol{J}$, has the following form:

$$\boldsymbol{J}(x,y)=\left[J_x(y)\hat{\boldsymbol{x}}+J_y(y)\hat{\boldsymbol{y}}\right]e^{-jk_{x0}x} \quad (5)$$

where

$$k_{x0}=\beta-j\alpha \quad (6)$$

and $J_x(y)$ and $J_y(y)$ represent the transverse variations of the x- and y-directed currents, respectively. Transforming this current and substituting it into (2)–(4) reduces the two-dimensional current transforms to a one-dimensional transform. Taking the inverse Fourier transform yields

$$E_x(x,y,z)=\frac{1}{2\pi}\int_{-\infty}^{\infty}\tilde{G}_{xx}(k_{x0},k_y,z,z_0)\tilde{J}_x(k_y)\cdot e^{-j(k_{x0}x+k_yy)}\,dk_y+\frac{1}{2\pi}\int_{-\infty}^{\infty}\tilde{G}_{xy}(k_{x0},k_y,z,z_0)\cdot\tilde{J}_y(k_y)e^{-j(k_{x0}x+k_yy)}\,dk_y \quad (7)$$

$$E_y(x,y,z)=\frac{1}{2\pi}\int_{-\infty}^{\infty}\tilde{G}_{yx}(k_{x0},k_y,z,z_0)\tilde{J}_x(k_y)\cdot e^{-j(k_{x0}x+k_yy)}\,dk_y+\frac{1}{2\pi}\int_{-\infty}^{\infty}\tilde{G}_{yy}(k_{x0},k_y,z,z_0)\cdot\tilde{J}_y(k_y)e^{-j(k_{x0}x+k_yy)}\,dk_y \quad (8)$$

and

$$E_z(x,y,z)=\frac{1}{2\pi}\int_{-\infty}^{\infty}\tilde{G}_{zx}(k_{x0},k_y,z,z_0)\tilde{J}_x(k_y)\cdot e^{-j(k_{x0}x+k_yy)}\,dk_y+\frac{1}{2\pi}\int_{-\infty}^{\infty}\tilde{G}_{zy}(k_{x0},k_y,z,z_0)\cdot\tilde{J}_y(k_y)e^{-j(k_{x0}x+k_yy)}\,dk_y. \quad (9)$$

III. Derivation of Integral Equations

A. Thin Conducting Strips

For very thin superconducting or normally conducting strips, where the fields within the strip are approximately uniform, the tangential components of the electric field at the strip are given by

$$\boldsymbol{E}_t(x,y,z_0)=Z_s'\boldsymbol{J}(x,y) \quad (10)$$

where Z_s' is the surface impedance of the conductor, with units Ω/square, $\boldsymbol{J}$ is the equivalent surface current density, and the subscript t denotes the components tangent to the strip (i.e., the x and y components). The equivalent surface current, $\boldsymbol{J}$, is given by

$$\boldsymbol{J}=\int_0^t\boldsymbol{J}_v\,dz=\boldsymbol{J}_v t \quad (11)$$

where $\boldsymbol{J}_v$ is the uniform volume current density within the strip and t is the thickness of the strip. For a perfect conductor Z_s' is equal to zero. For nonperfect conductors, Z_s' is approximated as [2]

$$Z_s'=\frac{E_{t_i}}{\int_0^t J_{v_i}\,dz}=\frac{1}{\sigma t},\qquad i=x \text{ or } y \quad (12)$$

where σ is the conductivity of the strip conductor. This conductivity is real for normal conductors and complex ($\sigma=\sigma_1-j\sigma_2$) for superconductors. Equation (12) is appropriate when the field variation within the strip is small.

To derive an integral equation in terms of the unknown surface current, $\boldsymbol{J}$, we enforce the boundary condition

(10) by testing it with a vector testing function $\boldsymbol{F}(y)$:

$$\int_{-\infty}^{\infty} \boldsymbol{E}_t(x,y,z_0)\cdot\boldsymbol{F}(y)\,dy = Z_s'\int_{-\infty}^{\infty}\boldsymbol{J}(x,y)\cdot\boldsymbol{F}(y)\,dy. \tag{13}$$

By alternately defining $\boldsymbol{F}(y)$ as $J_x^*(y)\hat{\boldsymbol{x}}$ and $J_y^*(y)\hat{\boldsymbol{y}}$, and substituting (7) and (8) into (13), we obtain the following set of coupled integral equations:

$$\int_{-\infty}^{\infty}\left[\tilde{G}_{xx}(k_{x0},k_y,z_0)-Z_s'\right]\tilde{J}_x(k_y)\tilde{J}_x^*(k_y)\,dk_y + \int_{-\infty}^{\infty}\tilde{G}_{xy}(k_{x0},k_y,z_0)\tilde{J}_y(k_y)\tilde{J}_x^*(k_y)\,dk_y = 0 \tag{14}$$

and

$$\int_{-\infty}^{\infty}\left[\tilde{G}_{yy}(k_{x0},k_y,z_0)-Z_s'\right]\tilde{J}_y(k_y)\tilde{J}_y^*(k_y)\,dk_y + \int_{-\infty}^{\infty}\tilde{G}_{yx}(k_{x0},k_y,z_0)\tilde{J}_x(k_y)\tilde{J}_y^*(k_y)\,dk_y = 0. \tag{15}$$

In these expressions $\tilde{J}^*$ is the conjugate of $\tilde{J}$, and $\tilde{G}_{ij}(k_{x0},k_y,z_0)$ is used to denote $\tilde{G}_{ij}(k_{x0},k_y,z_0,z_0)$.

B. Thick Conducting Strips

For thicker strips, where the thickness, t, is greater than a few skin depths, δ, or effective penetration depths, $\lambda_{\text{eff}}(T)$, the approximate boundary condition on the surface of the strip is given by

$$\boldsymbol{E}_t(x,y,z^{t,b}) = Z_s\boldsymbol{J}^{t,b}(x,y) \tag{16}$$

where $\boldsymbol{J}^t$ and $\boldsymbol{J}^b$ are the surface currents on the top and bottom surfaces of the strip and Z_s is the classical plane wave surface impedance:

$$Z_s = \frac{E_{t_i}}{\int_0^{\infty} J_{v_i}\,dz} = \left[\frac{j\omega\mu}{\sigma}\right]^{1/2}, \qquad i = x \text{ or } y. \tag{17}$$

In this expression J_v decreases exponentially with distance z into the conductor. If the thickness of the strip is small compared with the other dimensions of the structure, z^t and z^b, the positions of the top and bottom surfaces of the strip, respectively, can be approximated as z_0 (the middle of the strip). Thus, the currents $\boldsymbol{J}^t$ and $\boldsymbol{J}^b$ are collapsed into an equivalent surface current $\boldsymbol{J}(\boldsymbol{J}=\boldsymbol{J}^t+\boldsymbol{J}^b)$. However, a difficulty in deriving an integral equation in terms of $\boldsymbol{J}$ directly from (16) is that the right-hand side does not involve the equivalent current $\boldsymbol{J}$, but rather $\boldsymbol{J}^t$ and $\boldsymbol{J}^b$, depending upon whether the observation point is located on the top or bottom of the strip. Only in the special case where the current on the bottom (top) side of the strip is much greater than that on the top (bottom), where $\boldsymbol{J}$ is approximately equal to the current on the bottom (top), can we obtain an integral equation by directly enforcing the boundary condition (16) on the bottom (top) surface of the strip.

In order to model the strip as an equivalent surface current at z_0, an effective surface impedance, Z_s^e, must be used. The boundary condition then becomes

$$\boldsymbol{E}_t(x,y,z_0) = Z_s^e\boldsymbol{J}(x,y) \tag{18}$$

where $\boldsymbol{E}_t$ is the field produced by the equivalent surface current, $\boldsymbol{J}$.

To determine the effective surface impedance, the complex power dissipated by the equivalent current sheet should be the same as that for the actual strip conductor. The complex power for the equivalent current sheet is

$$P_c = \frac{1}{2}\int_S \boldsymbol{E}_t(x,y)\cdot\boldsymbol{J}^*(x,y)\,dS \tag{19}$$

where S denotes the surface of the equivalent current sheet. Using (18), this becomes

$$P_c = \frac{1}{2}Z_s^e\int_S \boldsymbol{J}(x,y)\cdot\boldsymbol{J}^*(x,y)\,dS. \tag{20}$$

Next, consider the actual strip conductor having different surface currents on the top and bottom surfaces of the strip. If it is assumed that the functional form of the current is the same on the top and bottom surfaces of the strip, with only an amplitude difference, the top and bottom surface currents are related as

$$\boldsymbol{J}^t(x,y) = \psi\boldsymbol{J}(x,y) \tag{21}$$

$$\boldsymbol{J}^b(x,y) = (1-\psi)\boldsymbol{J}(x,y) \tag{22}$$

where ψ is the ratio of the current on the top surface of the strip to the total surface current. The complex power dissipated by the actual strip is then

$$P_c = \frac{1}{2}Z_s\int_S \boldsymbol{J}^t(x,y)\cdot\boldsymbol{J}^{t*}(x,y)\,dS + \frac{1}{2}Z_s\int_S \boldsymbol{J}^b(x,y)\cdot\boldsymbol{J}^{b*}(x,y)\,dS \tag{23}$$

which may be written as

$$P_c = \frac{1}{2}pZ_s\int_S \boldsymbol{J}(x,y)\cdot\boldsymbol{J}^*(x,y)\,dS \tag{24}$$

where

$$p = \psi^2 + (1-\psi)^2. \tag{25}$$

Comparing (20) with (24), the effective surface impedance is determined as

$$Z_s^e = pZ_s. \tag{26}$$

For a general structure, one could obtain the factor p using a quasi-static technique or some other method. For the special case of a symmetric stripline, the currents on the top and bottom of the strip are equal, so that $\psi = 0.5$ and thus $p = 0.5$. Another limiting case is a microstrip transmission line where the strip is close to the ground plane. In this case $|\boldsymbol{J}^t| \ll |\boldsymbol{J}^b|$, so that $\psi \approx 0$ and $p \approx 1$.

An integral equation for the unknown equivalent surface current, $\boldsymbol{J}$, is derived by enforcing (18) using a testing

function, $\boldsymbol{F}(y)$, obtaining

$$\int_{-\infty}^{\infty} \boldsymbol{E}_t(x,y,z_0)\cdot\boldsymbol{F}(y)\,dy = pZ_s\int_{-\infty}^{\infty}\boldsymbol{J}(x,y)\cdot\boldsymbol{F}(y)\,dy. \tag{27}$$

By alternately defining $\boldsymbol{F}(y)$ as $J_x^*(y)\hat{\boldsymbol{x}}$ and $J_y^*(y)\hat{\boldsymbol{y}}$ and substituting (7) and (8) into (27), we obtain the following set of coupled integral equations:

$$\int_{-\infty}^{\infty}\left[\tilde{G}_{xx}(k_{x0},k_y,z_0)-pZ_s\right]\tilde{J}_x(k_y)\tilde{J}_x^*(k_y)\,dk_y + \int_{-\infty}^{\infty}\tilde{G}_{xy}(k_{x0},k_y,z_0)\tilde{J}_y(k_y)\tilde{J}_x^*(k_y)\,dk_y = 0 \tag{28}$$

and

$$\int_{-\infty}^{\infty}\left[\tilde{G}_{yy}(k_{x0},k_y,z_0)-pZ_s\right]\tilde{J}_y(k_y)\tilde{J}_y^*(k_y)\,dk_y + \int_{-\infty}^{\infty}\tilde{G}_{yx}(k_{x0},k_y,z_0)\tilde{J}_x(k_y)\tilde{J}_y^*(k_y)\,dk_y = 0. \tag{29}$$

These expressions are consistent with those obtained directly from (10) when $p=1$ and $Z_s' = Z_s$.

In this investigation we will assume that the width of the conducting strip is small compared with the wavelength; thus, the y component of the surface current will be neglected. With this assumption, (28) and (29) are reduced to the following integral equation:

$$\int_{-\infty}^{\infty}\left[\tilde{G}_{xx}(k_{x0},k_y,z_0)-pZ_s\right]\tilde{J}_x(k_y)\tilde{J}_x^*(k_y)\,dk_y = 0. \tag{30}$$

Basic to this analysis is the derivation of the dyadic Green's function, $\bar{\boldsymbol{G}}$, which represents the electric field in the mth layer caused by an arbitrarily oriented, unit strength Hertzian electric dipole, also in the mth layer. For this discussion, from (30), we note that only the $\hat{x}\hat{x}$ component is required. To formulate the electric field Green's function, Maxwell's equations are transformed, via a pair of Fourier transformations, into a pair of scalar transmission line equations. These transmission line expressions are solved by enforcing the boundary conditions at each interface separating the layers. This approach, often referred to as the spectral domain immittance method, has been presented in detail by others [6], [7] and will not be presented here. In the Appendix, $\tilde{G}_{xx}$ is presented in its final form.

IV. Method of Moments

The integral equation (30) is solved using the method of moments. In this procedure the transverse current variation $J_x(y)$ is approximated by

$$J_x(y) \approx \sum_{n=1}^{N} c_n J_{xn}(y) \tag{31}$$

where the c_n's are constant expansion coefficients and the J_{xn}'s are expansion (basis) functions. Using this expansion, (30) is approximated as

$$\sum_{n=1}^{N} c_n\int_{-\infty}^{\infty}\left[\tilde{G}_{xx}(k_{x0},k_y,z_0)-pZ_s\right]\cdot\tilde{J}_{xm}^*(k_y)\tilde{J}_{xn}(k_y)\,dk_y = 0, \qquad m=1,2,\cdots,N \tag{32}$$

where $\tilde{J}_{xt}(k_y)$ is the Fourier transform of the expansion function $J_{xt}(y)$. This equation is rewritten in the following matrix form:

$$\bar{\boldsymbol{Z}}\boldsymbol{C} = \boldsymbol{0} \tag{33}$$

where each element of the $N\times N$ matrix $\bar{\boldsymbol{Z}}$ is defined as

$$Z_{mn} = \int_{-\infty}^{\infty}\left[\tilde{G}_{xx}(k_{x0},k_y,z_0)-pZ_s\right]\tilde{J}_{xm}^*(k_y)\tilde{J}_{xn}(k_y)\,dk_y \tag{34}$$

and $\boldsymbol{C}$ is an $N\times 1$ vector containing the expansion coefficients. For nontrivial solutions of $\boldsymbol{C}$, the matrix $\bar{\boldsymbol{Z}}$ must be singular. Hence, the propagation constant k_{x0} is determined by solving

$$\det[\bar{\boldsymbol{Z}}] = 0. \tag{35}$$

The solution of this equation is obtained by employing a complex root finding algorithm, such as the secant method or Muller's method. The solutions for k_{x0} are assumed to produce fields which are bounded in the directions transverse to the direction of propagation; thus, the search is restricted to the region $k_{\max}^{gw} \leqslant k_{x0}$, where $k_{\max}^{gw}$ is the largest wavenumber for the guided-wave modes of this background structure [8]. This condition implicitly assumes that there is no loss (i.e., real wavenumbers). A small amount of loss results in complex wavenumbers which are simply perturbations of the lossless values; therefore, the prescribed search region still provides an appropriate start for the root finding algorithm. This condition also ensures that the poles of $\tilde{G}_{xx}$ lie along the imaginary k_y axis in the lossless case; hence, the integration path in (34) is performed along the real k_y axis. Once the modal propagation constant has been found, we determine the normalized current distribution by assigning one of the current coefficients (c_t) equal to unity and solving for the remaining c_n's by solving the resulting $(N-1)\times(N-1)$ matrix equation which results from (33).

In this investigation, dominant mode propagation is assumed, so that $J_x(y)$ is an even function about $y=0$. The basis function is chosen as a pair of symmetric pulses, with

$$J_{xn}(y) = \begin{cases} 1/w, & (y_n - w/4N) \leqslant |y| \leqslant (y_n + w/4N) \\ 0, & \text{otherwise} \end{cases} \tag{36}$$

where w is the width of the strip and $y_n = w(2n-1)/4N$. The Fourier transform of these offset pulses is given by

$$\tilde{J}_{xn}(k_y) = \frac{\cos(y_n k_y)}{wk_y/4}\sin\left(\frac{wk_y}{4N}\right). \tag{37}$$

Because of reciprocity, the $\bar{\boldsymbol{Z}}$ matrix is symmetric. Furthermore, because the basis functions are defined as pairs of single pulses, the elements of the $\bar{\boldsymbol{Z}}$ matrix can be

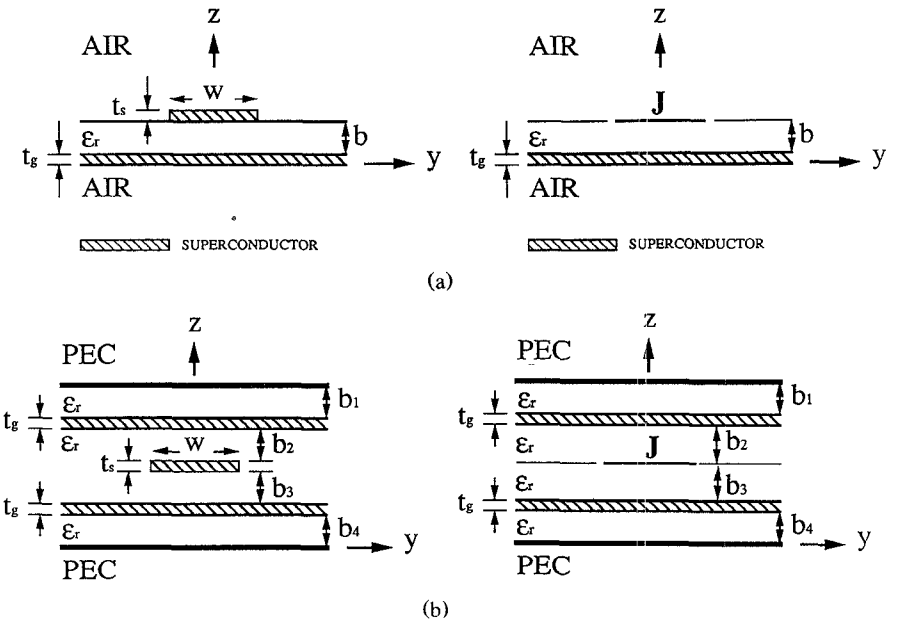

Fig. 2. Superconducting transmission lines and equivalent model geometries used in the present analysis: (a) microstrip and (b) stripline.

easily constructed from the $2N$ distinct Z_{mn} values which are obtained from (34) when using single pulse functions for $J_{xn}(y)$ and $J_{xm}(y)$. These $2N$ distinct values correspond to the $2N$ distinct separations $\Delta y = (n-1)w/(2N)$ $(n = 1 \cdots 2N)$ between centers of the individual pulses.

V. Two-Fluid Model

Since the exact mechanisms for high-temperature superconductivity have yet to be conclusively determined, there are no macroscopic theories which describe the electrical properties of these materials below their critical temperature, T_c. The models which are most commonly used for the low-temperature materials, the Mattis–Bardeen equations and the two-fluid model, have been applied to the high-temperature superconductors with varying degrees of success. At the present time, the simpler, two-fluid model seems to be more applicable to these new materials in weak magnetic fields, and will be used in this presentation. In our discussion, the magnetic fields are assumed to be weak enough that the flux is excluded from the interior of the superconductor (superconducting state). This model is readily extended, for slightly stronger magnetic fields, into the *mixed state* (partial penetration of magnetic flux) by adjusting the model parameters. However, for stronger magnetic fields, such that the superconductor is well within the mixed state, the simple two-fluid model breaks down. In this region, for high-T_c superconductors, an accurate model has not been developed.

The complex conductivity obtained from the two-fluid model is expressed as

$$\sigma = \sigma_n \left(\frac{T}{T_c}\right)^4 - j\left(\frac{1}{\omega\mu\lambda_{\text{eff}}^2(0)}\right)\left(1-(T/T_c)^4\right) \quad (38)$$

where σ_n is associated with the normal state conductivity at T_c and $\lambda_{\text{eff}}(T)$ is the effective field penetration depth as a function of temperature, T, in degrees kelvin. There are wide variances for these model parameters from sample to sample, and the temperature and frequency characteristics of these quantities have not been conclusively determined. The effective penetration depths are generally greater than calculated London penetration depths for the high-T_c materials owing to irregularities such as crystalline anisotropy and misalignment, grain boundaries, impurities, and other phases of the superconducting material. The effects of other loss mechanisms, such as grain boundary losses and residual losses, are often included in σ_n. Despite these uncertainties the two-fluid model is still a powerful empirical tool and gives important qualitative results.

VI. Numerical Results

We will demonstrate the effectiveness of our general stripline and microstrip model by considering the slow wave propagation of the dominant quasi-TEM modes along these structures. The geometries that we will consider are shown in Fig. 2. These structures are used since they are nearly identical to the microstrips and striplines that are commonly used to experimentally determine the electrical properties of thin-film superconductors. In these test structures, the superconducting thin films are deposited on several substrates, which are then sandwiched together, as shown in the figure, to produce the final transmission line. On occasion, normal conductors (e.g. Cu, Au, and Ag) or low-temperature superconductors (such as Nb) are used. In these situations, two-sided deposition is possible and the substrate materials are often different from those for the high-T_c superconduc-

tors. The formulation presented in the previous sections is capable of analyzing these multiple-layer transmission lines. In Fig. 2 we show diagrams of actual stripline and microstrip geometries, with strip conductors of finite thickness, t_s, alongside the models for these geometries used in this analysis. In these model geometries the strip is represented by an equivalent surface current, $\boldsymbol{J}$, of width w as discussed previously. From extensive comparisons with rigorous solutions for infinitely wide, finite thickness strip models, we have determined that the proper location for the surface current, $\boldsymbol{J}$, is such that the distances between the ground planes and the strip surface, b in Fig. 2(a) and b_2 and b_3 in Fig. 2(b), are maintained. These modeling requirements are particularly important for very thin transmission line structures. Examples of the comparison with infinitely wide strip models will be shown later. In addition, for the remainder of our discussion we will assume that the thickness of each superconductor layer is equal to t; therefore, $t_g = t_s = t$.

To simplify our present discussion, we will neglect all the losses associated with the dielectrics in the transmission line. It is true that for good superconducting thin-film devices the total loss in the actual structure is often dominated by the losses of the dielectric. For these examples, however, we are primarily interested in determining the phase velocity of the dominant mode, which is only weakly dependent upon this additional loss. In these examples, the phase velocity is computed as $v_p = \omega/\beta$, where β is the real part of the complex propagation constant k_{x0}.

For the examples to be presented, we have determined, through extensive numerical experimentation, that it is necessary to use only a single pulse basis function to represent the transverse variation of the current for narrow strips. Furthermore, in these examples, the superconducting strips are very thin; therefore, Z_s' defined by (12) is used in (30) with $p = 1$. Unless otherwise specified, the parameters for the two-fluid model will be those for a typical laser ablated $YBa_2Cu_3O_7$ thin film, where $\lambda_{\text{eff}}(0) = 1500$ Å, $\sigma_n = 2\times 10^5$ S/m, and $T_c = 90$ K. Also, the temperature will be assumed to be 70 K and the substrate materials are assumed to be $LaAlO_3$ with a dielectric constant of 23.

To begin, we will compare the slow wave propagation results obtained with our rigorous spectral-domain analysis for a thin superconducting microstrip transmission line (Fig. 2(a)) with those obtained by Swihart's infinitely wide strip model [1]. For this example, the width of the strip, w, is equal to 10^{-3} m and the substrate thickness is equal to the thickness of the superconducting ground plane and strip ($b = t$). The normalized phase velocities as a function of layer thickness, t, obtained from these models are shown in Fig. 3. The computed phase velocities are normalized by the factor $c/\sqrt{\epsilon_r}$, where c is the velocity of light in free space and ϵ_r is the dielectric constant of the substrate material, which is 23. This figure clearly demonstrates the *slowing* of the phase velocity of the dominant

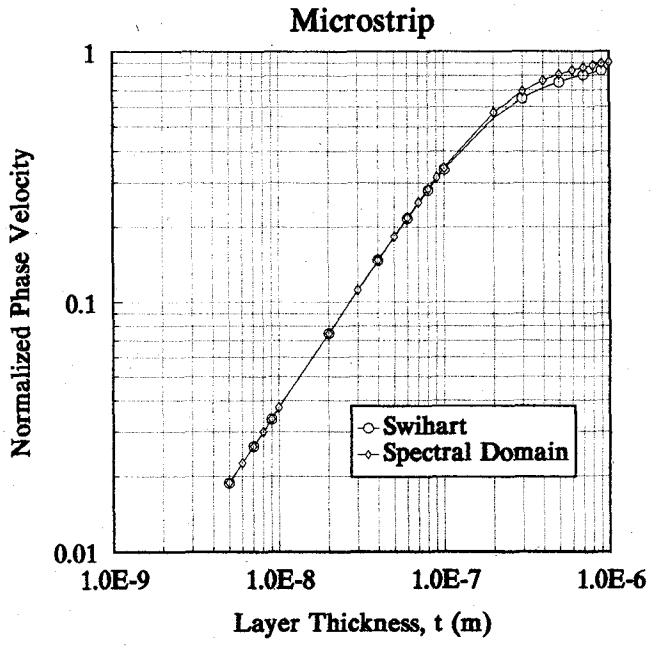

Fig. 3. Comparison between present spectral-domain analysis and infinite-strip-width model of Swihart [1] for a superconducting microstrip transmission line. Model parameters: $b = t$, $w = 10^{-3}$ m, and $\epsilon_r = 23$ (Fig. 2(a)).

microstrip transmission line mode caused by the kinetic inductance associated with the superconducting current. As the dimensions of the structure and the thicknesses of the superconducting layers decrease, the fractional amount of magnetic energy stored in the superconductors increases, thereby, decreasing the phase velocity. The two models agree very well up to $t \approx 10^{-7}$ m, where the results start to diverge. This separation is due, primarily, to two effects. First, the microstrip is dispersive; thus the effective dielectric constant (phase velocity) of the structure, neglecting the kinetic inductance effects, varies with strip width, w. This effect is not included in Swihart's model. Second, the surface impedance Z_s' given by (12), used to model the material characteristics of the thin strip in the spectral-domain formulation, starts to break down when the fields within the strip depart substantially from uniform. This occurs as the thickness of the strip approaches the effective penetration depth, $\lambda_{\text{eff}}(T)$:

$$\lambda_{\text{eff}}(T) = \lambda_{\text{eff}}(0)\left[1-(T/T_c)^4\right]^{-1/2}. \qquad (39)$$

For this example $(T/T_c = 70\text{ K}/90\text{ K}$ and $\lambda_{\text{eff}}(0) = 1500$ Å) $\lambda_{\text{eff}}(70\text{ K}) = 2.2\times 10^{-7}$ m.

In Fig. 4 the effects of varying the width of this microstrip line are presented. We notice that the strip width does affect the phase velocity, but these effects are due primarily to the line dispersion, which is not related to the conducting materials. This effect is manifest as the lateral displacement of the individual responses. The spreading of the curves as the layer thickness is decreased is a result of the different kinetic inductance contributions for the strips of different width. For this geometry ($b \ll w$), it is readily apparent that the phase velocity of the structure is

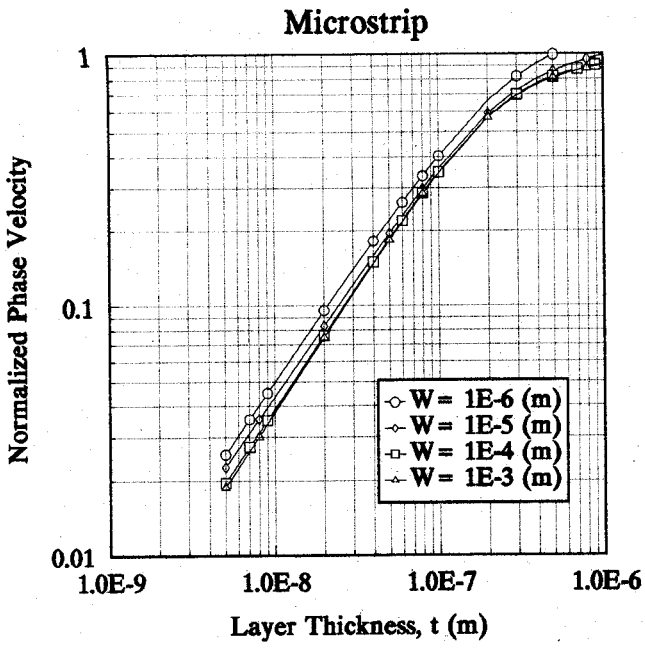

Fig. 4. Effect of strip width on the normalized phase velocity ($v_p\sqrt{\epsilon_r}/c$) for the high-T_c superconducting microstrip line of Fig. 3. Model parameters: $b = t$ and $\epsilon_r = 23$.

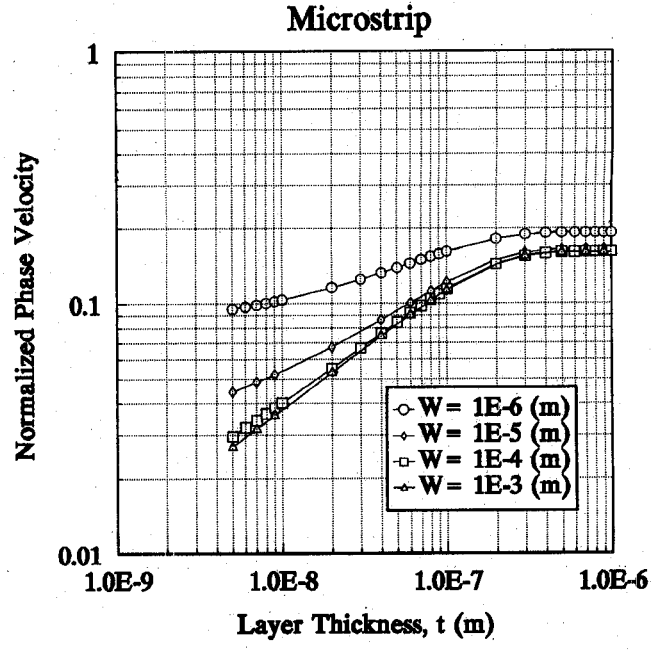

Fig. 6. Effect of strip width on the normalized phase velocity ($v_p\sqrt{\epsilon_r}/c$) of the microstrip used for Fig. 4 with a PEC strip ($Z_s = 0$) and a high-T_c ground plane. Model parameters: $b = 5\times10^{-9}$ m and $\epsilon_r = 23$.

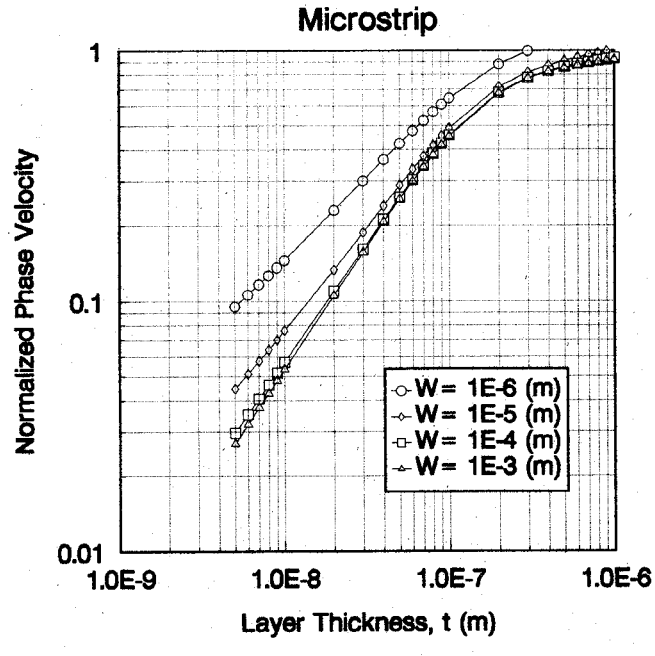

Fig. 5. Effect of strip width on the normalized phase velocity ($v_p\sqrt{\epsilon_r}/c$) of the microstrip used for Fig. 4 with a PEC strip ($Z_s = 0$) and a high-T_c ground plane. Model parameters: $b = t$ and $\epsilon_r = 23$.

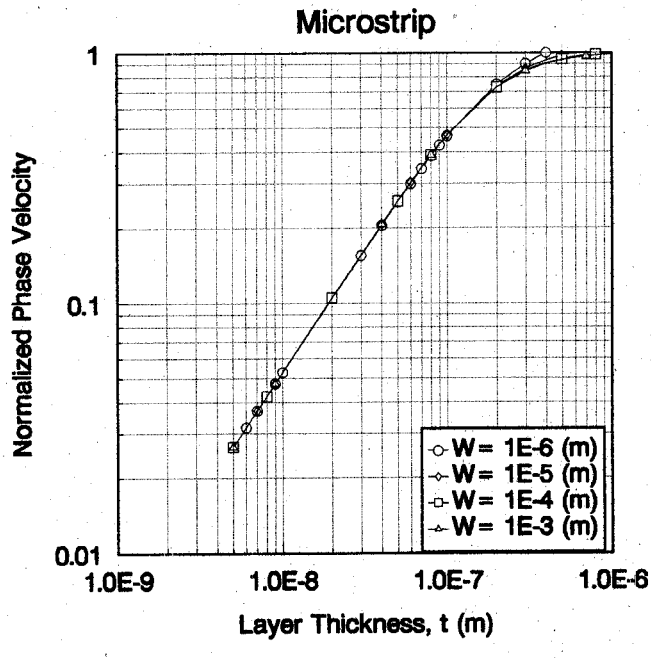

Fig. 7. Effect of strip width on the normalized phase velocity ($v_p\sqrt{\epsilon_r}/c$) of the microstrip used for Fig. 4 with a thin high-T_c strip and a PEC ground plane. Model parameters: $b = t$ and $\epsilon_r = 23$.

a very weak function of the width of the microstrip line. In order to separate the effects of the superconducting strip and the superconducting ground plane on the phase velocity, consider the plots shown in Figs. 5, 6, and 7. To generate these plots, the microstrip geometry of the previous example (Figs. 3 and 4) is used with the following modifications: for the responses shown in Figs. 5 and 6, the strip is a perfect electric conductor (PEC, $Z_s = 0$), while the ground plane remains a superconductor, and for Fig. 7, the strip is a thin superconductor and the ground plane is a PEC. As we see from Fig. 5, the kinetic inductance contributions from the superconducting ground plane do vary appreciably with strip width. This results in a decreasing phase velocity with increasing strip width. For this geometry ($w/b \gg 1$), the sensitivity of the phase velocity to the PEC strip width is related to the penetration of the fields through the superconductor into

the dielectric *backing* the ground plane. For wide strips, the response agrees with that predicted by the infinitely wide strip model [1]; however, as the strip width decreases the effects of the penetration through the ground plane decrease. This is demonstrated in Fig. 6, which shows the phase velocity for the microstrip geometry used for Fig. 5, except that the substrate thickness is fixed at 5×10^{-9} m. As the thickness of the superconducting ground plane is increased the phase velocity increases, as expected; however, the dependence upon the strip width decreases. For thick ground planes ($t > \lambda_{\text{eff}}$), the only width effect is, apparently, that due to dispersion. Also notice that the resulting phase velocities are significantly faster than those for the corresponding completely superconducting microstrip (Fig. 4). However, when only the strip is superconducting, as shown in Fig. 7, the phase velocity is nearly independent of the strip width, and agrees well with that predicted by the infinitely wide strip model [1]. Therefore, we conclude that for extremely thin ($b \leqslant \lambda_{\text{eff}}$) microstrip transmission lines, for which $w/b \gg 1$, the dependence of the phase velocity on the strip width is significant only when there is penetration through the ground plane. When the ground plane is PEC, there is essentially no variation with the strip width for these wide strips. Since this width dependence is related to the penetration through the ground plane, we expect that larger penetration depths will cause the phase velocities in Figs. 4 and 5 to increase even more with decreasing strip width. Also, for these microstrip lines, the phase velocity increases as the strip width decreases, which is opposite to the behavior exhibited when using narrower strips on thicker substrates. This effect will be discussed later using a stripline example.

In Fig. 8, we demonstrate how the effective penetration depth affects the phase velocity of the microstrip line used in the previous examples. For this example, the strip width is taken to be 10^{-4} m. As these results indicate, the phase velocity of the dominant mode along an extremely thin microstrip line is a strong function of $\lambda_{\text{eff}}(T)$. This property is often used to determine λ_{eff} from transmission line measurements [3], [9]. From the previous results, we observe that the effect of the strip width is small for these thin structures, where $b \leqslant \lambda_{\text{eff}}$ and $w/b \gg 1$; therefore, only small errors will be produced if it is not accounted for in the determination of λ_{eff}.

In Fig. 9, we compare the slow wave propagation results obtained from our spectral-domain analysis of a thin superconducting stripline transmission line (Fig. 2(b)) with those obtained by using the transverse resonance method, which is based on transmission line techniques similar to those discussed in the Appendix, to rigorously model the stripline with an infinitely wide center strip of finite thickness (Triplate model). The transverse resonance method is used to find the dominate odd TM mode propagation constant, from which the phase velocity is obtained [10]. For this comparison, the width of the strip is equal to 1×10^{-3} m, $b_2 = b_3 = 1.5t$, and $b_1 = b_4 = 20$ mils (5.1×10^{-4} m). The dielectric constant for the substrates and ground plane backing layers is 23. This figure shows the slowing of the phase velocity as the layer thickness is decreased, and it also demonstrates the excellent agreement between our stripline model and the rigorous model for the stripline with an infinitely wide, finite-thickness center conductor.

The results of Figs. 4–8 for the microstrip are repeated, in Figs. 10–14, for a similar stripline transmission line

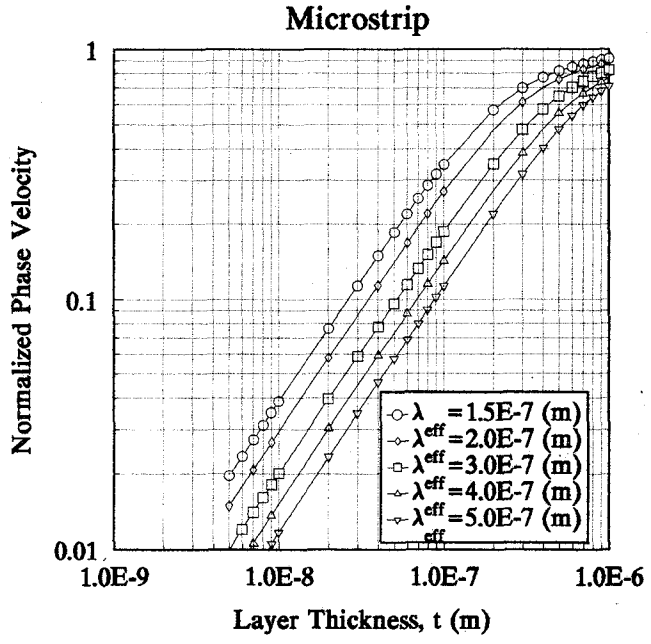

Fig. 8. Effect of $\lambda_{\text{eff}}(T)$ on the normalized phase velocity ($v_p\sqrt{\epsilon_r}/c$) for the high-T_c superconducting microstrip line of Fig. 4. Model parameters: $b = t$, $\epsilon_r = 23$, and $w = 10^{-4}$ m.

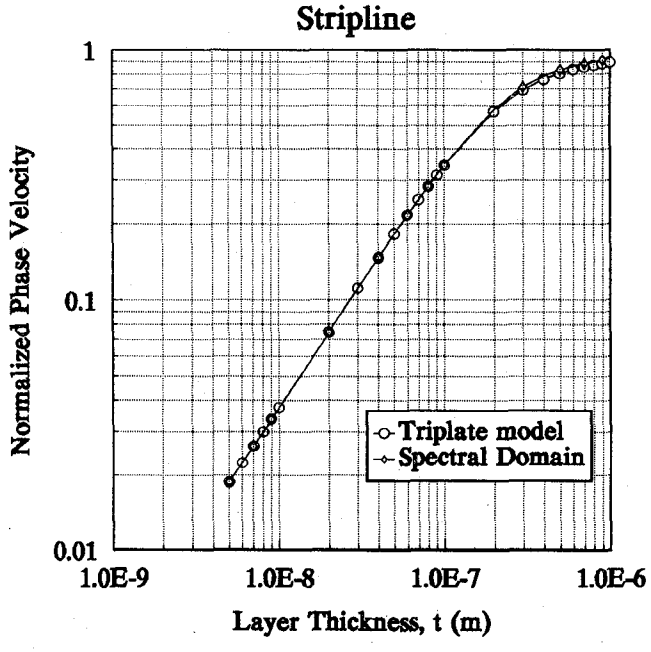

Fig. 9. Comparison between present spectral-domain analysis and infinite-strip-width model (Triplate model) for a superconducting stripline transmission line. Model parameters: $b_2 = b_3 = 1.5t$, $b_1 = b_4 = 20$ mils, $w = 10^{-3}$ m, and $\epsilon_r = 23$ (Fig. 2(b)).

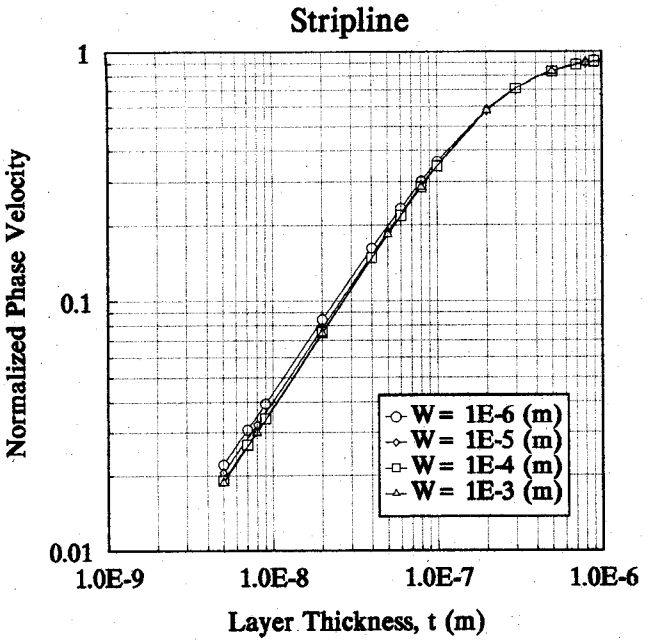

Fig. 10. Effect of strip width on the normalized phase velocity ($v_p\sqrt{\epsilon_r}/c$) for the high-T_c superconducting stripline of Fig. 2(b). Model parameters: $b_2 = b_3 = 1.5t$ and $\epsilon_r = 23$.

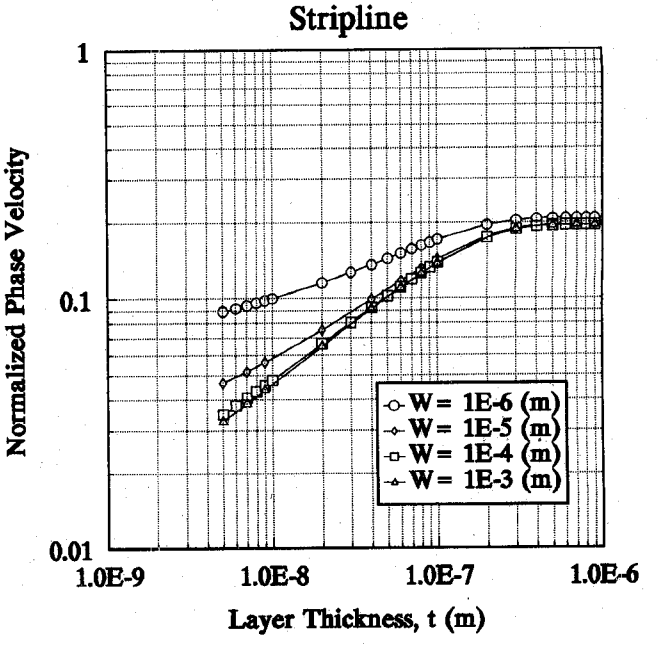

Fig. 12. Effect of strip width on the normalized phase velocity ($v_p\sqrt{\epsilon_r}/c$) for the stripline used for Fig. 10 with a PEC strip ($Z_s = 0$) and high-T_c ground planes. Model parameters: $b_2 = b_3 = 7.5\times10^{-9}$ m and $\epsilon_r = 23$.

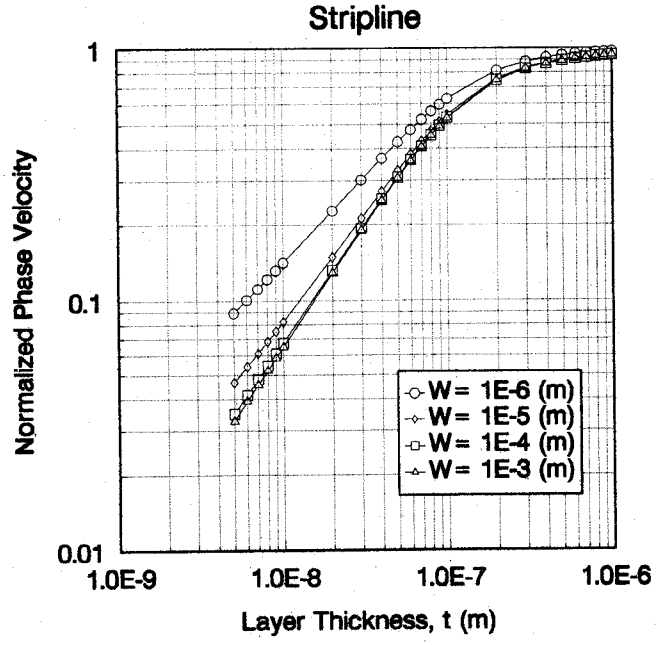

Fig. 11. Effect of strip width on the normalized phase velocity ($v_p\sqrt{\epsilon_r}/c$) for the stripline used for Fig. 10 with a PEC strip ($Z_s = 0$) and high-T_c ground planes. Model parameters: $b_2 = b_3 = 1.5t$ and $\epsilon_r = 23$.

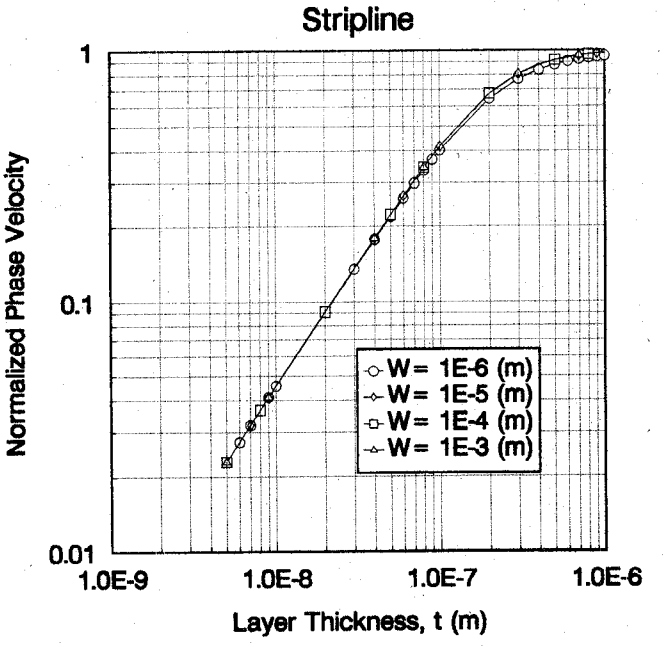

Fig. 13. Effect of strip width on the normalized phase velocity ($v_p\sqrt{\epsilon_r}/c$) for the stripline used for Fig. 10 with a thin high-T_c strip and PEC ground planes. Model parameters: $b_2 = b_3 = 1.5t$ and $\epsilon_r = 23$.

(Fig. 2(b)). For this stripline, $b_2 = b_3 = 1.5t$, where t is the thickness of the superconducting ground planes and strip, and $b_1 = b_4 = 20$ mils. The only apparent difference between the microstrip and stripline responses is that the stripline has very little dispersion; therefore, the phase velocity, neglecting the effects of the kinetic inductance, does not change with strip width, w, unless there is penetration through the ground planes (as in Figs. 11 and 12). Also, the phase velocities for the stripline are slightly slower than those of the microstrip, owing to the additional superconducting ground plane.

A difficulty presently associated with obtaining such slow phase velocities in the laboratory is associated with the construction of high-T_c superconducting microstrips and striplines of such small dimensions. The commonly used $LaAlO_3$ substrates are very brittle and must be on the order of 10–20 mils thick to survive the necessary

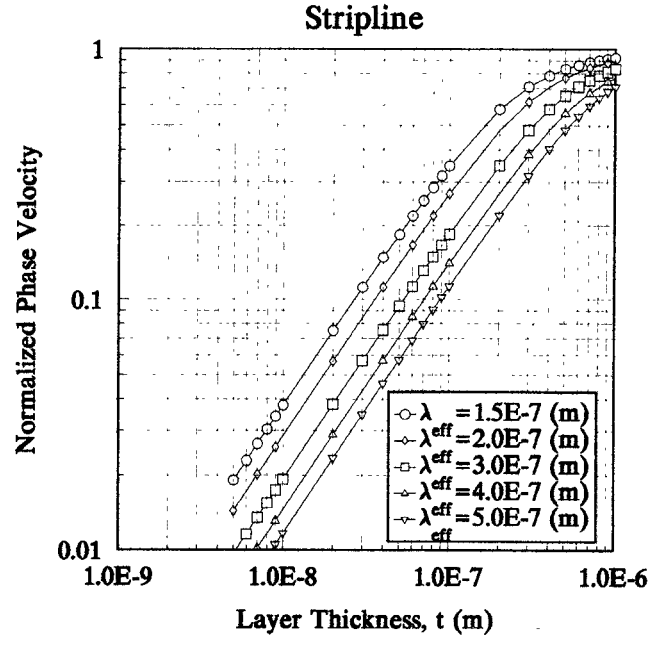

Fig. 14. Effect of $\lambda_{\text{eff}}(T)$ on the normalized phase velocity $(v_p\sqrt{\epsilon_r}/c)$ for the high-T_c superconducting stripline of Fig. 10. Model parameters: $b_2 = b_3 = 1.5t$, $\epsilon_r = 23$, and $w = 10^{-4}$ m.

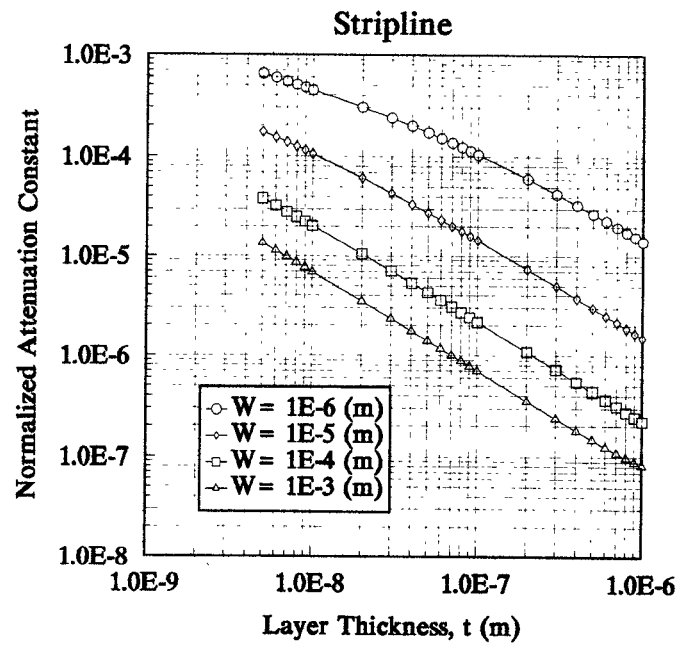

Fig. 16. Effect of strip width on the normalized attenuation constant (α/k_0) for the high-T_c superconducting stripline of Fig. 2(b). Model parameters: $b_2 = b_3 = 20$ mils and $\epsilon_r = 23$.

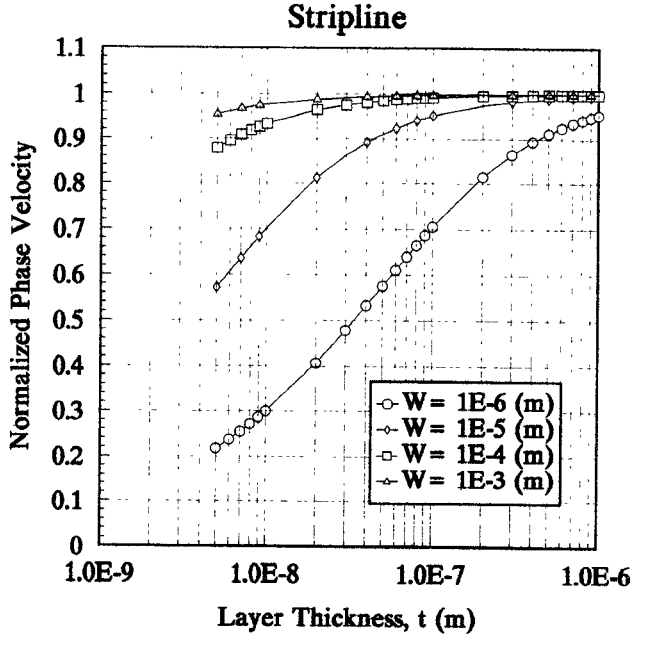

Fig. 15. Effect of strip width on the normalized phase velocity $(v_p\sqrt{\epsilon_r}/c)$ for the high-T_c superconducting stripline of Fig. 2(b). Model parameters: $b_2 = b_3 = 20$ mils and $\epsilon_r = 23$.

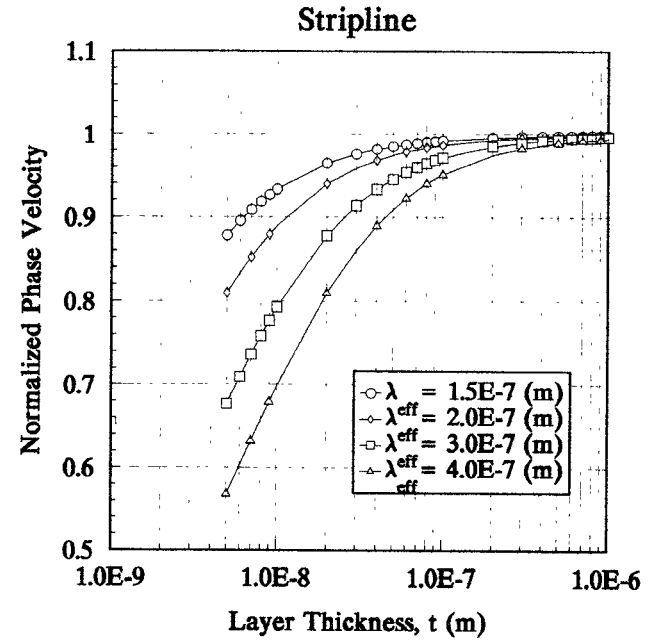

Fig. 17. Effect of $\lambda_{\text{eff}}(T)$ on the normalized phase velocity $(v_p\sqrt{\epsilon_r}/c)$ for the high-T_c superconducting stripline of Fig. 2(b). Model parameters: $b_2 = b_3 = 20$ mils, $\epsilon_r = 23$, and $w = 10^{-4}$ m.

mechanical stresses received in the deposition process and in the device construction. Infinite-width strip models predict a negligible amount of slowing for transmission lines of these dimensions. However, as the strip width is reduced, substantial reductions in the phase velocity occur. This is demonstrated in Fig. 15 for a stripline with dimensions $b_1 = b_2 = b_3 = b_4 \equiv b = 20$ mils $(5.1 \times 10^{-4}$ m) and superconducting ground planes and strip thicknesses equal to t. The substrate is assumed to be $LaAlO_3$ ($\epsilon_r =$ 23). (For the remainder of this section we will present results only for striplines; however, the results are directly applicable to similarly constructed microstrip lines.) The corresponding attenuation constants, normalized by the free-space wavenumber, k_0, are shown in Fig. 16. In this example the phase velocity is a very strong function of the strip dimensions, particularly for the cases where $w/b \ll 1$. For these thicker structures the effect of penetration through the ground planes is minimal. Also, as expected,

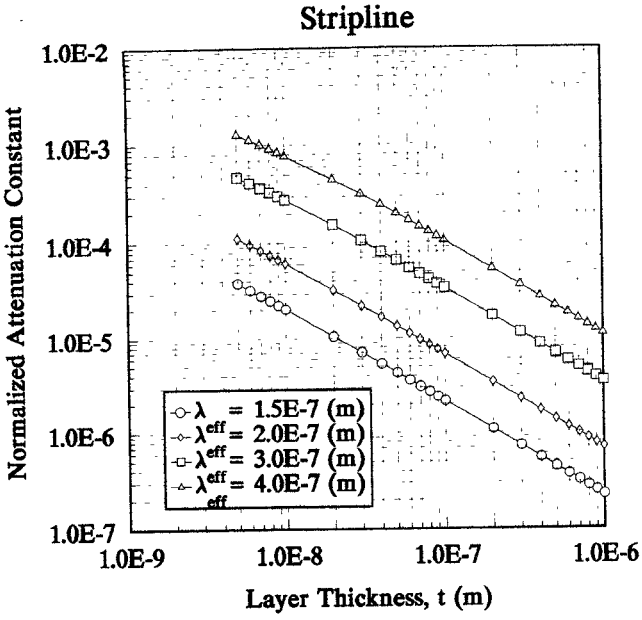

Fig. 18. Effect of $\lambda_{\text{eff}}(T)$ on the normalized attenuation constant (α/k_0) for the high-T_c superconducting stripline of Fig. 2(b). Model parameters: $b_2 = b_3 = 20$ mils, $\epsilon_r = 23$, and $w = 10^{-4}$ m.

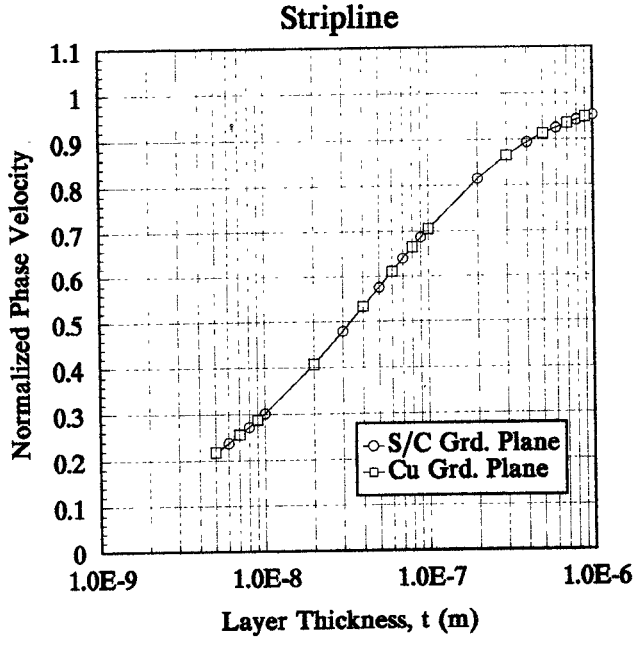

Fig. 19. Comparison of normalized phase velocity $(v_p\sqrt{\epsilon_r}/c)$ for the stripline of Fig. 15 having either high-T_c superconducting or copper ground planes. Model parameters: $b_2 = b_3 = 20$ mils, $\epsilon_r = 23$, $w = 10^{-4}$ m, and $\sigma_{\text{Cu}} = 5.8\times10^7$ S/m. For both cases the strip thickness is equal to t. For the superconducting case, the ground plane thickness is t, and for the copper case, the ground plane thickness is fixed at 20 mils.

the attenuation constant increases as the strip width decreases. Again, recall that dielectric losses have been neglected in these examples. The corresponding plots for a fixed strip width ($w = 10^{-4}$ m) and variable λ_{eff} are shown in Figs. 17 and 18. Appreciable changes in the phase velocity occur for the range of λ_{eff} shown, and the attenuation increases dramatically as the penetration depth increases.

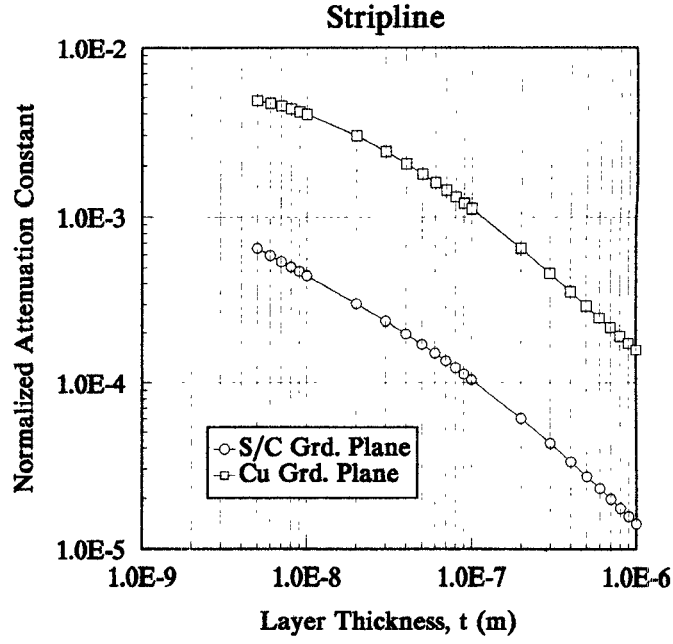

Fig. 20. Comparison of normalized attenuation constant (α/k_0) for the stripline of Fig. 15 having either high-T_c superconducting or copper ground planes. Model parameters: $b_2 = b_3 = 20$ mils, $\epsilon_r = 23$, $w = 10^{-4}$ m, and $\sigma_{\text{Cu}} = 5.8\times10^7$ S/m. For both cases the strip thickness is equal to t. For the superconducting case, the ground plane thickness is t, and for the copper case the ground plane thickness is fixed at 20 mils.

The dependence of the phase velocity on the electrical characteristics of the strip, for $w/b \ll 1$, is demonstrated by comparing the $w = 10^{-6}$ m response in Figs. 15 and 16 with that for the equivalent stripline with the superconducting ground planes replaced by 20-mil-thick copper ($\sigma = 5.8\times10^7$ S/m) ground planes. This comparison is shown in Figs. 19 and 20. Note that the phase velocity is effectively independent of the ground plane characteristics for this stripline geometry since $w/b \ll 1$; yet, the attenuation constant increases by nearly an order of magnitude owing to the copper ground planes. For such a narrow strip, assuming that the strip and the ground planes have the same surface resistance, the relative contribution to the total loss is much higher for the strip than it is for the ground planes. However, since in this example the surface resistance of the superconductor is much smaller than that of the copper, the use of copper ground planes increases the total loss dramatically.

VII. Conclusions

We have presented a rigorous spectral-domain formulation for the analysis of arbitrary multilayered stripline and microstrip transmission lines. This formulation is used to determine the complex modal propagation constants of the structure, from which the phase velocity, attenuation constant, and Q of the transmission line can be determined. Although derived in general, these techniques are applied to analyze transmission lines constructed either totally or partially of superconducting materials. The characteristics of the superconductors are incorporated into the analysis via the two-fluid model. Several numeri-

cal examples are presented which demonstrate slow wave propagation along superconducting microstrip and stripline transmission lines. We observed how field penetration through the superconducting ground planes may have an influence on the phase velocity when the separation between the strip and the ground planes is less than λ_{eff} and much less than the strip width. For thicker substrates, particularly when the strip width is smaller than the strip to ground plane separation, the effects of field penetration through the ground planes are minimal. We have also demonstrated that it is possible to achieve significant slow wave behavior for thick-substrate transmission lines by using sufficiently small strip widths.

This formulation is sufficiently general to accurately model actual stripline and microstrip transmission lines used to characterize high-temperature superconducting thin films. By correlating these modeling results with measurements, we can determine many of the macroscopic electrical parameters and develop improved models for the high-T_c materials.

Appendix

Using the *spectral-domain immittance method* [6], [7], we obtain the $\hat{x}\hat{x}$ component of the electric field dyadic Green's function for an arbitrarily oriented, unit strength Hertzian electric dipole, assuming that the source and observation points are in the same layer (mth layer), as [8]

$$\tilde{G}_{xx}(z) = -\frac{k_x^2}{k_t^2}\tilde{G}^{V^{\text{TM}}}(z,z') - \frac{k_y^2}{k_t^2}\tilde{G}^{V^{\text{TE}}}(z,z') \quad \text{(A1)}$$

where $k_t^2 = k_x^2 + k_y^2$. The voltage Green's functions $\tilde{G}^{V^{\text{TE}}}$ and $\tilde{G}^{V^{\text{TM}}}$ are given as follows (with superscripts TE and TM suppressed):

$$\tilde{G}^V(z,z') = \frac{Z_m}{2}\left(e^{-jk_{zm}|z-z'|} + \tilde{Q}_m^V(z,z')\right) \quad \text{(A2)}$$

where

$$\tilde{Q}_m^V(z,z') = \frac{1}{D_m}\Big(\Gamma_m^d e^{-jk_{zm}[(z+z')-2z_m]} + \Gamma_{m-1}^u e^{-jk_{zm}[2z_{m-1}-(z+z')]} + 2\Gamma_m^d\Gamma_{m-1}^u \cdot e^{-j2k_{zm}(z_{m-1}-z_m)}\cos\left[k_{zm}(z-z')\right]\Big) \quad \text{(A3)}$$

and

$$D_m = 1 - \Gamma_m^d\Gamma_{m-1}^u e^{-j2k_{zm}(z_{m-1}-z_m)} \quad \text{(A4)}$$

with $k_{zm} = (k_m^2 - k_t^2)^{1/2}$, where k_m is the wavenumber in layer m. The reflection coefficients Γ_m^d and Γ_m^u are given by

$$\Gamma_m^d = \frac{Z_m^d - Z_m}{Z_m^d + Z_m}, \qquad m = 1,2,\cdots,M \quad \text{(A5)}$$

and

$$\Gamma_m^u = \frac{Z_m^u - Z_{m+1}}{Z_m^u + Z_{m+1}}, \qquad m = 1,2,\cdots,M \quad \text{(A6)}$$

where M is the total number of layers. From transmission line theory, the impedances Z_m^d and Z_m^u are given by

$$Z_m^d = Z_{m+1}\frac{Z_{m+1}^d + jZ_{m+1}\tan\Phi_{m+1}}{Z_{m+1} + jZ_{m+1}^d\tan\Phi_{m+1}}, \qquad m = M-1, M-2,\cdots,1 \quad \text{(A7)}$$

and

$$Z_m^u = Z_m\frac{Z_{m-1}^u + jZ_m\tan\Phi_m}{Z_m + jZ_{m-1}^u\tan\Phi_m}, \qquad m = 2,3,\cdots,M \quad \text{(A8)}$$

where $\Phi_m = k_{zm}(z_{m-1} - z_m)$. The wave impedances $Z_m = Z_m^{\text{TE}}$ or Z_m^{TM} are given by

$$Z_m^{\text{TM}} = \frac{k_{zm}}{\omega\epsilon_m} \quad \text{(A9)}$$

and

$$Z_m^{\text{TE}} = \frac{\omega\mu_m}{k_{zm}}. \quad \text{(A10)}$$

References

[1] J. C. Swihart, "Field solution for a thin-film superconducting strip transmission line," *J. Appl. Phy.*, vol. 32, no. 3, pp. 461–469, 1961.

[2] J. M. Ponds, C. M. Krowne, and W. L. Carter, "On the application of complex resistive boundary conditions to model transmission lines consisting of very thin superconductors," *IEEE Trans. Magn.*, vol. 37, no. 1, pp. 181–189, 1989.

[3] J. M. Ponds, J. H. Claassen, and W. L. Carter, "Measurements and modeling of kinetic inductance microstrip delay lines," *IEEE Trans. Microwave Theory Tech.*, vol. MTT-35, pp. 1256–1262, Dec. 1987.

[4] G. Arfken, *Mathematical Methods For Physicists*. New York: Academic Press, 1970, pp. 681–683.

[5] R. F. Harrington, *Time-Harmonic Electromagnetic Fields*. New York: McGraw-Hill, 1961, pp. 458–459.

[6] L. B. Felsen and N. Marcuvitz, *Radiation and Scattering of Waves*. Englewood Cliffs, NJ: Prentice-Hall, 1973, pp. 183–222.

[7] T. Itoh and W. Menzel, "A full-wave analysis for open microstrip structures," *IEEE Trans. Antennas Propagat.*, vol. AP-29, no. 1, pp. 63–68, 1981.

[8] D. Nghiem, "Analysis of proper and improper modes on a multiple-layer stripline," M.S. thesis, Dept. Elec. Eng., Univ. of Houston, 1990.

[9] W. H. Henkels and C. J. Kircher, "Penetration depth measurements on type II superconducting films," *IEEE Trans. Magn.*, vol. 13, no. 1, pp. 63–66, 1977.

[10] J. M. Ponds, P. Weaver, and I. Kaufman, "Propagation characteristics of inductively coupled superconducting microstrip," in *1989 IEEE MTT Int. Microwave Symp. Dig.*, 1989, vol. 1, pp. 451–454.

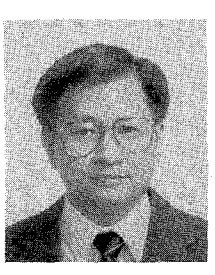

David Nghiem (S'90) was born in Gia Dinh, Vietnam, on April 13, 1960. He received the B.S.E.E. degree from Texas A&M University, College Station, TX, in 1985 and the M.S. degree in electrical engineering in 1990 from the University of Houston, Houston, TX, where he is currently a doctoral student in the area of electromagnetics. Since 1987 he has been a Teaching Assistant and Research Assistant in the Department of Electrical Engineering. His present interests include guided-wave problems, leaky-wave antennas, and the characterization and application of high-temperature superconductors.

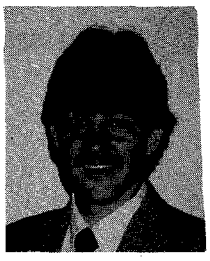

Jeffery T. Williams (S'85–M'87) was born in Kula, Maui, Hawaii, on July 24, 1959. He obtained the B.S., M.S., and Ph.D. degrees in electrical engineering from the University of Arizona, Tucson, in 1981, 1984, and 1987, respectively.

He was a design engineer at the Zonge Engineering and Research Organization, Tucson, AZ, from 1981 to 1982. In 1982, he was a summer engineer at the Lawrence Livermore National Laboratory, Livermore, CA. During the years 1983–1986 he served as a summer scientist at the Schlumberger-Doll Research Center, Ridgefield, CT. He has been an Assistant Professor in the Electrical Engineering Department at the University of Houston, Houston, TX, since 1987. His present research interests include antenna design and measurements, characterization and applications of high-temperature superconductors, computational electromagnetics, microstrip and stripline wave-guiding structures, and high-frequency measurement techniques.

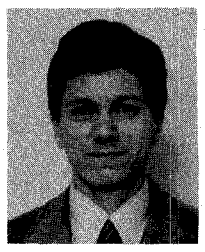

David R. Jackson (S'83–M'85) was born in St. Louis, MO, on March 28, 1957. He obtained the B.S.E.E. and M.S.E.E. degrees from the University of Missouri, Columbia, in 1979 and 1981, respectively, and the Ph.D. degree in electrical engineering from the University of California, Los Angeles, in 1985.

He is currently an Assistant Professor in the Department of Electrical Engineering at the University of Houston, Houston, TX. His research interests at present include microstrip and leaky-wave antennas for microwave and millimeter-wave applications, guided-wave problems, and computer-aided design of microstrip structures.